



Method for Measuring Thermal Conductivity of Small Samples Having Very Low Thermal Conductivity

*Robert A. Miller and Maria A. Kuczmariski
Glenn Research Center, Cleveland, Ohio*

NASA STI Program . . . in Profile

Since its founding, NASA has been dedicated to the advancement of aeronautics and space science. The NASA Scientific and Technical Information (STI) program plays a key part in helping NASA maintain this important role.

The NASA STI Program operates under the auspices of the Agency Chief Information Officer. It collects, organizes, provides for archiving, and disseminates NASA's STI. The NASA STI program provides access to the NASA Aeronautics and Space Database and its public interface, the NASA Technical Reports Server, thus providing one of the largest collections of aeronautical and space science STI in the world. Results are published in both non-NASA channels and by NASA in the NASA STI Report Series, which includes the following report types:

- **TECHNICAL PUBLICATION.** Reports of completed research or a major significant phase of research that present the results of NASA programs and include extensive data or theoretical analysis. Includes compilations of significant scientific and technical data and information deemed to be of continuing reference value. NASA counterpart of peer-reviewed formal professional papers but has less stringent limitations on manuscript length and extent of graphic presentations.
- **TECHNICAL MEMORANDUM.** Scientific and technical findings that are preliminary or of specialized interest, e.g., quick release reports, working papers, and bibliographies that contain minimal annotation. Does not contain extensive analysis.
- **CONTRACTOR REPORT.** Scientific and technical findings by NASA-sponsored contractors and grantees.

- **CONFERENCE PUBLICATION.** Collected papers from scientific and technical conferences, symposia, seminars, or other meetings sponsored or cosponsored by NASA.
- **SPECIAL PUBLICATION.** Scientific, technical, or historical information from NASA programs, projects, and missions, often concerned with subjects having substantial public interest.
- **TECHNICAL TRANSLATION.** English-language translations of foreign scientific and technical material pertinent to NASA's mission.

Specialized services also include creating custom thesauri, building customized databases, organizing and publishing research results.

For more information about the NASA STI program, see the following:

- Access the NASA STI program home page at <http://www.sti.nasa.gov>
- E-mail your question via the Internet to help@sti.nasa.gov
- Fax your question to the NASA STI Help Desk at 443-757-5803
- Telephone the NASA STI Help Desk at 443-757-5802
- Write to:
NASA Center for AeroSpace Information (CASTI)
7115 Standard Drive
Hanover, MD 21076-1320



Method for Measuring Thermal Conductivity of Small Samples Having Very Low Thermal Conductivity

*Robert A. Miller and Maria A. Kuczmariski
Glenn Research Center, Cleveland, Ohio*

National Aeronautics and
Space Administration

Glenn Research Center
Cleveland, Ohio 44135

Trade names and trademarks are used in this report for identification only. Their usage does not constitute an official endorsement, either expressed or implied, by the National Aeronautics and Space Administration.

This work was sponsored by the Fundamental Aeronautics Program at the NASA Glenn Research Center.

Level of Review: This material has been technically reviewed by technical management.

Available from

NASA Center for Aerospace Information
7115 Standard Drive
Hanover, MD 21076-1320

National Technical Information Service
5285 Port Royal Road
Springfield, VA 22161

Available electronically at <http://gltrs.grc.nasa.gov>

Method for Measuring Thermal Conductivity of Small Samples Having Very Low Thermal Conductivity

Robert A. Miller and Maria A. Kuczmariski
National Aeronautics and Space Administration
Glenn Research Center
Cleveland, Ohio 44135

Abstract

This paper describes the development of a hot plate method capable of using air as a standard reference material for the steady-state measurement of the thermal conductivity of very small test samples having thermal conductivity on the order of air. As with other approaches, care is taken to ensure that the heat flow through the test sample is essentially one-dimensional. However, unlike other approaches, no attempt is made to use heated guards to block the flow of heat from the hot plate to the surroundings. It is argued that since large correction factors must be applied to account for guard imperfections when sample dimensions are small, it may be preferable to simply measure and correct for the heat that flows from the heater disc to directions other than into the sample. Experimental measurements taken in a prototype apparatus, combined with extensive computational modeling of the heat transfer in the apparatus, show that sufficiently accurate measurements can be obtained to allow determination of the thermal conductivity of low thermal conductivity materials. Suggestions are made for further improvements in the method based on results from regression analyses of the generated data.

Introduction

Thermal conductivity is a physical property of fundamental importance to the developers of highly insulating materials. Standard techniques for its direct steady-state measurement, which were greatly influenced by a long history of test development at national laboratories [1-13], have been established. In the majority of cases described in the literature for measuring low thermal conductivity samples (on the order of the thermal conductivity of air), the sample size must be large, varying from a few hundred centimeters to over a meter. However, researchers involved in the development of advanced, highly insulating materials often develop new materials in small batches. Therefore, test samples may only be available in sizes too small for the methods normally used to directly measure thermal conductivity. Papers describing a National Institute of Standards and Technology (NIST)-sponsored test development effort from the late 1990s addressed this need, emphasizing materials used for building insulation [14,15]. At the National Aeronautics and Space Administration (NASA) Glenn Research Center, the focus is on the development of materials, such as those based on aerogels [16].

Techniques for precisely measuring steady-state thermal conductivity are much more complex than they may initially appear. In principle, the thermal conductivity of an insulator can be measured by placing a thin sample of an unknown material between two plates—one heated and the other cooled—and measuring the electrical power required to attain a temperature gradient across a sample of known thickness. However, all the power coming from the heater does not automatically go into the sample, and the sample does not necessarily experience one-dimensional heat flow with parallel heat flux vectors through it. This is especially true for very low conductivity samples, where insulation around the edge of the sample could have thermal conductivity comparable to that of the sample. Early in the last century, it was recognized [17] that it was highly desirable to surround the disc and sample assembly with temperature-controlled “guards” designed to block the flow of heat in directions other than into the sample and to insure that the flow of heat through the sample is essentially one-dimensional. Even with considerable care, this “guarded hot plate” approach is still imperfect and requires theoretical, and often

experimental, corrections for imperfections in design, especially for measurements on low thermal conductivity insulators.

There are two general types of guarded hot plate techniques. The first type, represented by ASTM C177-04 [2] and ISO 8302:1991 [3], is an absolute method where the apparatus is constructed in such a way that thermal conductivity may be directly obtained from measurement of electrical power, temperatures, and sample dimensions. The other type, represented by ASTM C518-04 [4] and ISO 8301:1991 [5], incorporates one or more heat flux meters in the stack of plates calibrated against standard samples whose conductivity was previously measured using the absolute approach.

These four standards have many features in common. They all rely on a meter plate surrounded by a guard plate—both of which are electrically heated and set to the same temperature. A gap separates the two plates. In two-sided designs, matched sample plates are placed on each side of the meter- and guard-plates. In the single-sided design, the sample is only placed against one side of the meter- and guard-plates. Some sort of insulation and another heated guard are used in place of the second specimen. The size of the plates is envisioned to be 0.1 to 1 m diameter or square, with the smaller size being more appropriate for isotropic samples. A “similarly constructed” chill plate is placed on the far side of the sample or samples. The stack of heater-, sample-, and chilled plates may be oriented vertically or horizontally. The heated- and chilled-plates are preferably constructed from a high thermal conductivity metal, with electrical heaters arranged so as to insure that the plates are isothermal to within $\pm 0.1\text{K}$. The temperatures of the plates may be measured using two or more thermocouples or other temperature sensors. The simplest approach uses fine thermocouples to measure the temperatures of the plates, which are assumed to be the temperatures on each side of the sample. However, this approach assumes that there is essentially zero contact resistance between the sample and the plates. The standards permit using compliant spacers between the sample and the plates to minimize contact resistance or, if the sample itself is compliant, a small amount of sample compression. For samples so compliant that they would crush under the load of the clamping force holding the stack together, spacers are allowed to prevent crushing. The standards call for treating the surface of the heated and cooled plates so as to give them high emissivity. This would ensure that a fraction of the available heat flux is available as radiation, in addition to the heat transfer by conduction. The standards also call for cylindrical guards—with axial gradient preferably matching the gradient of the stack—surrounding the entire assembly. Because the entire apparatus must achieve near-perfect thermal equilibrium, the standards note that hours or even days may be required to achieve thermal equilibrium.

The standards stress three major points. First, great care must be taken to mathematically and experimentally correct for imperfections in design, including the effect of the gap between the meter plate and the guard plate and “edge heat flows at the periphery of the sample”. Second, no one design is appropriate for every situation; every design must be considered on a case-by-case basis. Finally, the standards are not intended to be restrictive; research into new approaches is encouraged.

ASTM E1225-04 [6] is similar to the previous techniques in that it uses a standard material that is placed on one or both sides of the test sample whose conductivity is being measured, and employs heater and cooler discs with cylindrical guard surrounding the entire assembly. It differs in that this guard may have an axial gradient matching the axial gradient of the stack of plates or be isothermal with a temperature equal to the mean temperatures of the test sample. The space between the walls of the cylindrical guard and the stack are filled with powdered insulation. This technique is intended for test samples having a thermal conductivity no lower than 0.2 W/m-K , which is much greater than the thermal conductivity of air (about 0.026 W/m-K at room temperature).

There is one case in the literature that considers the development of a guarded hot plate apparatus for very small, very low thermal conductivity materials. Flynn and Gorthala presented two papers in the late 1990s [14, 15] describing how, using great care, such an apparatus could have been constructed. The work was conducted under a Small Business Innovative Research (SBIR) Phase I contract from NIST. They designed a small guarded hot plate apparatus for determining the thermal conductivity of very small samples, $1\text{ to }3\text{ cm}^2$, with a thickness as high as 1.3 cm . It was to cover a temperature range of at least $-40\text{ to }10\text{ }^\circ\text{C}$ in an environment of air, selected gases, or vacuum. The primary conductivity range was

designed to be from 0.02 to 0.05 W/m-K, and, if possible, from less than 0.005 to 0.35 W/m-K. The accuracy was to have been less than 5 percent (less than 2 percent near 25 °C), and the repeatability was to have been less than 2 percent (less than 0.5 percent near 25 °C). The meter and guard on the cold plate side were designed to have a heat flux meter. Interestingly, ceramic material was being considered for the meter and guard plates (hot and cold). These materials—which included BeO, AlN, Si, or polycrystalline diamond—were considered because their heating approach required an electrical insulator. The surfaces of the plates were to have been treated so that they had high emittance or possibly, in some cases, treated to match the emittance corresponding to the end use of the material being tested, Flynn and Gorthala argued in favor of a single-sided guarded hot plate approach that was much smaller than any other device available for measuring materials having very low thermal conductivity. The authors noted that constructing such a small guarded hot plate apparatus required serious correction—especially involving heat flow across the gap. The sample thickness should scale down in proportion to the way the lateral dimensions have been scaled down (in apparent contradiction to the stated goal of allowing up to 1.3 cm thick samples). They favored an absolute measurement approach and noted the general lack of calibration standards for highly insulating materials. They also expressed skepticism for using air as a calibration standard [14, 15].

This apparatus was to have been of direct value to manufacturers of insulation materials and polymers, particularly for use in characterizing experimental products that are only available in very small sample sizes. The prototype was to have been built if a Phase II SBIR contract had been awarded. However, no evidence was found in the literature to indicate that the apparatus had been built and tested.

Finally, when considering the use of air as a standard reference material, it is instructive to consider the use of the guarded hot plate approach for measuring the thermal conductivity of a gas. The approach of Michels, et al. [18-21] used highly polished copper plates with silica coating to prevent tarnishing. The spacing between plates was 0.409 or 1.275 mm. Small temperature differences between plates of 0.006 and 0.4 °C were employed (presumably because they were studying the effect of fine temperature differences about the critical point of carbon dioxide). This procedure allowed them to make accurate measurements of carbon dioxide thermal conductivity.

In this study, we considered the possibility of using an alternative approach for the steady-state measurement of the thermal conductivity of small samples having very low thermal conductivity. The approach attempts to measure, rather than shut down, the flow of heat in directions other than through the sample. We envision using the apparatus for screening at room temperature, although, in principle, it could be extended down to lower temperatures using suitable cryogenic coolants. Materials showing promise in the screening test could be fabricated in large quantities and tested by a more standard hot-plate approach, or perhaps the liquid nitrogen boil-off cryostat approach [22-24] where a cryogenic fluid is placed in a vessel that has been insulated with the low thermal conductivity material of interest and the time before all of the fluid boiled off is recorded.

This technique requires that a standard reference material be used. An example of a standard reference material having relatively low thermal conductivity is Glass Fiberboard SRM 1450c [1], which has a thermal conductivity of about 0.033 W/m-K at room temperature. As supplied, its thickness is 25 mm. However, because of its layered structure, it may not lend itself well for machining into small, well-characterized samples. Expanded polystyrene EPS SRM 1453 [1] is another standard reference material with similar thermal conductivity and similar difficulty in machining into samples of about 4 mm in thickness. Because of the relative lack of small standard reference materials having very low thermal conductivity, we examine whether air can be used as a small reference standard with as much or greater accuracy and greater simplicity than available solid materials.

Experimental Design

The experimental data was obtained from an apparatus that consists of an electric resistance heated copper disc 0.0254 m (1 in.) in diameter by 0.00476 m (3/16 in.) thick. A second identically-sized copper disc is cooled using chilled water. Adopting the low emissivity approach of Michels, et al. [18-21], both

opposing surfaces of the two copper discs are polished to a mirror finish using 4000 grit abrasive paper. A guard ring, made from strong, insulating polymethacrylimide (PMI) foam (Evonik Industries AG, Rohacell 71), is placed between the heater and chiller discs. The ring dimensions are 0.0254 m (1 in.) outside diameter, 0.01905 m (0.75 in.) inside diameter, and 0.004 m (0.159 in.) thick. The center of the PMI foam ring forms the test volume, and the ring itself acts as a temperature guard. The size of the test volume is, therefore, 0.01905 m (0.75 in.) diameter by 0.004 m (0.159 in.) thick. The features described above are shown in the center of Figure 1(a), which represents the version of the experimental apparatus used for the measurements described in this paper. A suggested future version of the device is shown in Figure 1(b), which will be discussed later in this paper. Matched thermocouples are used to measure the heater and chiller disc temperatures and the wall temperature. The thermocouples are not shown in the figure to prevent it from becoming excessively cluttered. The heater and chiller discs are each affixed to a larger disc of PMI foam. For the experimental part of this study, these discs are approximately 0.071 m (2.8 in.) diameter by 0.038 m (1.5 in.) thick. Three holes drilled near the edge of both of these discs accommodate nylon threaded rods used to provide a light clamping pressure on the heater disc/sample/chiller disc assembly. A partially compressed spring on each threaded rod helps to provide a uniform, gentle clamping pressure. The test assembly consists of the two large PMI foam discs, the heater and chiller discs, and the PMI foam ring/sample volume when clamped together. The stack consists of the heater disc, sample region along with the PMI foam ring, and the cooler disc.

The test assembly is placed inside of an aluminum cylinder 0.254 m (10 in.) long by 0.203 m (8 in.) diameter by 0.00318 m (1/8 in.) wall thickness. Copper cooling coils fed with water accurately maintained at a set temperature—typically 25 °C—are wrapped around the aluminum tube. The open ends of the aluminum tube are closed using foam and balsa wood, and chill plates are placed near the edge. These edge-chilled plates are fed with the same source of 25 °C water that feeds the coils to the wall. The cylinder sits on a water cooled base-plate, and an insulating box is placed over them both. Note that this aluminum cylinder is similar in principle to the isothermal guard option under ASTM E1225 [6]. However, rather than using a very low conductivity powder fill envisioned in that standard, we are attempting to use air, which also has a low thermal conductivity, but is safer and less messy. Care must be taken when using air to insure that convection does not greatly disturb the heat transfer.

A power supply provides the power to the heater disc. Two chillers are employed. One is set to 25 °C for the wall and environmental chamber temperatures, and the other supplies chilled water to the chiller disc. Water-to-air heat exchangers—commonly referred to as radiators—are placed in front of the air intakes for each chiller and cooled using the 25 °C chiller water. A pump built into the 25 °C chiller is

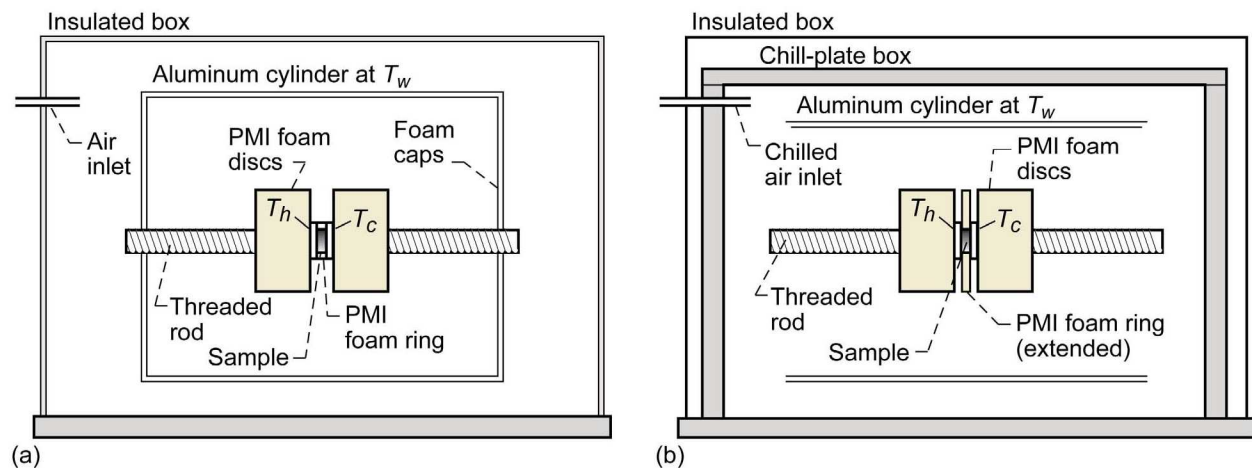


Figure 1.—Schematic of thermal conductivity apparatus. (a) Design used for the experiments described in this paper. (b) Potential future design where the outside diameter of the PMI foam ring is extended and the surrounding box is formed from six chill plates.

used to flow the water through the aluminum cylinder and the cylinder-end chill plates. A small hobby pump provides the flow to the heat exchangers, and a peristaltic metering pump provides the flow of the chilled water to the chilled disc of the test assembly.

The environment in which the apparatus is located is important. The room in which the apparatus sits must have low humidity such that its dew point is less than the temperature of the low temperature chiller. Otherwise, condensation could occur on the sample and apparatus. This is suggested by both the ASTM and ISO standards [2-6]. Dry air with a temperature equal to the wall temperature should be introduced into the volume around the apparatus. Water absorbed by the sample will change the measured thermal conductivity. Also, absorption of water by the PMI foam will change its thermal conductivity and, therefore, the calibration of the apparatus. At 15 percent relative humidity, PMI foam absorbs 1.2 percent water by weight; at 30 percent relative humidity, PMI foam absorbs 2.4 percent water by weight [25]. Finally, the temperature of the room should be controlled to within a few degrees to prevent fluctuations in the chiller temperature.

Computational Model

The computational fluid dynamics (CFD) code FLUENT (ANSYS, Inc.) [26] was used to model the apparatus. It uses a finite volume method to discretize the continuity, momentum, and energy equations. Equations may be solved alone or in combination.

An axisymmetric model was used. Figure 2 shows the various regions and boundary conditions in the model. The heater, cooler, and wall temperatures were varied in the model. Temperature ranges were 303.15 to 313.15 K for the heater, 283.15 to 293.15 K for the cooler, and 279.15 to 298.35 K for the wall. In each case investigated, the wall temperature was either equal to or approximately equal to the average of the heater and cooler disc temperatures. Aerogel, an extremely low thermal conductivity material [16], was used as the sample, and PMI foam was used as the insulating material around it.

The thermal conductivity of both the aerogel and PMI foam was expressed as:

$$k_{\text{aerogel,rohacell}} = Gk_{\text{air}} \quad (1)$$

where

k_{air} thermal conductivity of air (W/m-K)
 G constant (dimensionless)

The thermal conductivity of air was expressed as a function of temperature based on data from Holman [27]. The values for G were chosen to be 0.5, 1.0, and 1.5. $G = 1.0$ gives the thermal conductivity of air, 0.0261 W/m-K. This covered the range of expected aerogel thermal conductivities to be measured in the future. The heat capacity and density of air were also expressed as polynomial functions of temperature based on data in Holman [27]. The value of the thermal conductivity at room temperature for the grade of PMI foam used in this study was about 0.032 W/m-K. Because of its highly porous nature, it would contain mostly air; therefore, its thermal conductivity was allowed to vary with temperature in the same manner as air. This is confirmed by the product data [25]. The density and heat capacity of PMI foam were expressed as constants and obtained from information from the manufacture [25].

A second-order upwind scheme was used for both the momentum and energy equations, with an under-relaxation factor set to 0.7 for the momentum equation and 1 for the energy equation. The convergence criteria for the solutions were defined as scaled residuals below 1×10^{-3} for the momentum equation and 1×10^{-10} for the energy equation. Decreasing these values did not result in a change in the model predictions.

The sensitivity of the results to grid density was studied using three different grid densities that were based on the number of computational cells used across the sample. Figure 3 shows the grid density across the sample for the three grids used. A non-uniform grid was used over parts of the model to minimize the total number of computational cells. The maximum aspect ratio for the cells was 5:1.

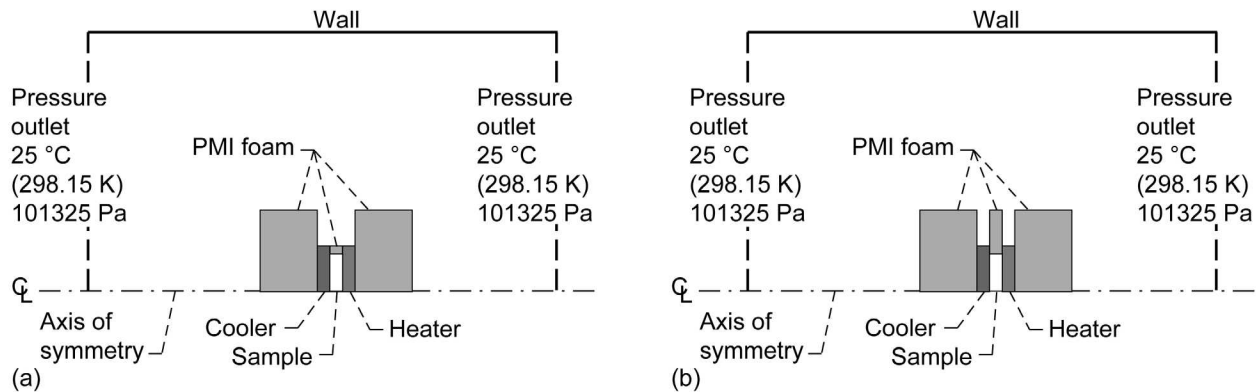


Figure 2.—Schematic of CFD model showing (a) the air gap case versus (b) the extended PMI foam case.

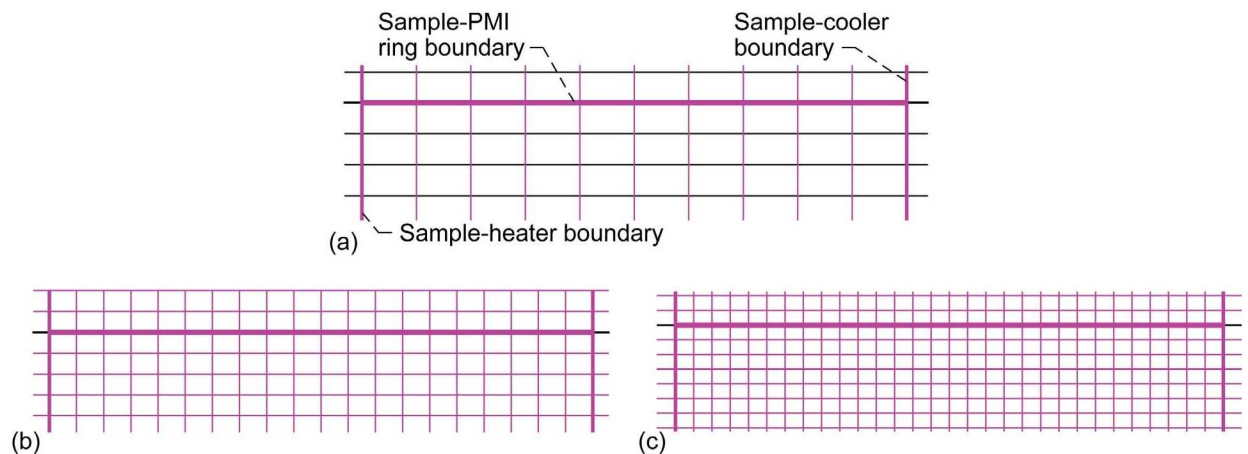


Figure 3.—Portion of grids near the edge of the sample investigated. (a) 10 cells across sample, (b) 20 cells across sample. (c) 30 cells across sample.

Table 1 shows the total number of computational cells used in each grid. The results showed that the grid based on 20 cells across the sample (grid 2) was sufficient to achieve grid-independent results. The difference in heat transferred across various internal boundaries was generally less than or equal to 1 percent between grids 2 and 3, with a maximum difference of less than 5 percent. Grid 2 was used for the rest of this study.

TABLE 1.—GRIDS USED IN SENSITIVITY STUDY

	Grid 1	Grid 2	Grid 3
Number of cells across sample	10	20	30
Number of cells in X-direction	134	242	370
Number of cells in Y-direction	76	142	204
Total number of cells in computational domain	210	384	574

The goal of this study was to examine the effects of convection and conduction; therefore, radiation was not included in the model. However, radiation effects will be considered below in a separate analysis.

Modeling Results

Extensive CFD modeling gave us a thorough understanding of the apparatus being constructed and guided its development and improvement. No attempt will be made to show all of the early concepts. This

discussion will focus on the latter stage of design, where modeling results gave direct insight into the apparatus performance.

A number of parameters proved useful in the analysis of the apparatus:

Q_{in}	heat entering sample from heater (W)
Q_{total}	total heat leaving heater disc (W)
k_{sample}	thermal conductivity of sample material (W/m-K)
l	sample thickness (m)
A	sample cross sectional area (m ²)
T_h	heater temperature (K)
T_c	cooler temperature (K)
T_w	wall temperature (K)

These quantities can be used to calculate the following:

$$\Delta T = T_h - T_c \text{ temperature difference across sample (K)} \quad (2)$$

$$Q_{1D} = \left(\frac{k_{sample}}{l} \right) A \Delta T \text{ one dimensional heat transfer (W)} \quad (3)$$

$$\frac{Q_{1D}}{Q_{in}} \text{ indicator of 1D heat flow (dimensionless)} \quad (4)$$

$$Q_{lost} = Q_{total} - Q_{1D} \text{ heat lost from sample} \\ \text{(heat that does not participate in the 1D heating of the sample) (W)} \quad (5)$$

$$T_{av} = \frac{T_h + T_c}{2} \text{ average temperature (K)} \quad (6)$$

The goal of this study was to determine how to construct an apparatus that could allow Q_{1D} (the heat directly related to the thermal conductivity) to be accurately extracted from Q_{total} (the measured heat). It was anticipated that their difference, Q_{lost} , would have to be obtained by calibration using a standard reference material of known conductivity. Furthermore, it was hoped that air could be used as a standard reference material. Several criteria had to be met for this approach to be feasible. First, the calibration at one value of thermal conductivity should apply at other values of the conductivity. Second, the quantity Q_{1D} should not be too small compared with Q_{total} . Third, the heat flow across the specimen should be close to one-dimensional.

Extensive modeling was used to determine if the above criteria could be met. An initial series of 108 CFD model runs was conducted that used various combinations of the three treatments of the gap region along the side of the stack, three values of ΔT , four values of sample thickness, and three values of sample thermal conductivity. The model provided four values of heat flow from each surface of the heater: 1) the major surface opposite the sample, Q_{op} , 2) the side of the heater, Q_{side} , 3) the heater into the PMI foam ring, Q_{ring} , and 4) the heater into the sample, Q_{in} .

Figure 4 is a plot comprised of 108 stacked bars, each divided into four segments. The various values of Q have been divided by ΔT . The combined height of each bar represents the modeled value of $\frac{Q_{total}}{\Delta T}$.

The length of the uppermost segment of each bar represents the modeled value of $\frac{Q_{in}}{\Delta T}$. For perfect one-dimensional flow, Q_{in} would be precisely equal to Q_{1D} . For imperfect, but nearly one-dimensional heat flow, they are approximately equal, i.e.:

$$Q_{in} \equiv Q_{1D} \quad (7)$$

and

$$Q_{lost} \equiv Q_{total} - Q_{in} \quad (8)$$

The combined height of the lower three stacked bars is a visual representation of Q_{lost} as defined by Eq. (8). The figure shows that there is essentially no difference in the height of each group of three bars; in fact, each takes on the appearance of a single wider bar. Since the three bars in each group represent the three values of sample thermal conductivity, Q_{lost} appears to be essentially independent of the sample's thermal conductivity. This implies that a calibration conducted at one thermal conductivity would hold over the entire range of interest, thus avoiding the iterative or recursive type of solution that would be necessary if the thermal conductivity also appeared as an independent variable. The figure also shows that

$\frac{Q_{lost}}{\Delta T}$ is insensitive to the value of ΔT —especially for the cases where the PMI foam is partially or fully extended into the gap region along the side of the stack. This means that Q_{lost} tends to vary in a linear manner with ΔT . In addition, there is an inverse relationship between $\frac{Q_{lost}}{\Delta T}$ and the sample thickness. This

relationship arises because the values of both $\frac{Q_{ring}}{\Delta T}$ and $\frac{Q_{side}}{\Delta T}$ show the same general behavior as $\frac{Q_{lost}}{\Delta T}$.

The heat leaving from the opposite side of the specimen, $\frac{Q_{op}}{\Delta T}$, is essentially independent of the modeled test variables.

We may now examine how the magnitude of Q_{in} compares to Q_{total} . Figure 4 shows that the ratio of Q_{in} (or, therefore, Q_{1D}) to Q_{total} increases as the sample conductivity increases, and that the ratio is higher for thinner samples. However, the ratio does not appear to be a function of ΔT for the second two geometries. For example, for the case of an extended PMI foam ring and a 3.8 mm thick sample, $\frac{Q_{in}}{Q_{total}}$ is 0.17 for a sample thermal conductivity half that of air, 0.29 for a sample thermal conductivity equals that of air, and 0.38 for a sample thermal conductivity 1.5 times that of air. In each case, the value of Q_{total} is not overwhelmingly greater than the value of Q_{1D} , implying that this approach with care may be used to accurately measure the thermal conductivity of small test samples of low thermal conductivity. However, this also means that the conductivity of more insulating materials will be subject to greater error. Therefore, Q_{total} must be determined with high precision, since even a one percent error in the determination of Q_{total} would multiply to an error in the measured conductivity of about 3 to 6 percent as thermal conductivity decreased from a higher to a lower value.

Figure 5 begins to explore the feasibility of using air as a calibration sample by examining whether the various $\frac{Q}{\Delta T}$ values are essentially the same for air and solid samples having the same thermal conductivity. This plot compares twelve air samples and twelve solid samples, all with the same thermal conductivity. The latter twelve are repeated from the previous plot. From the figure, it appears that the adjacent bars are essentially equal for all but the largest (6.4 mm) separation, especially when ΔT is not too large. This implied that air could possibly be used as a calibration standard.

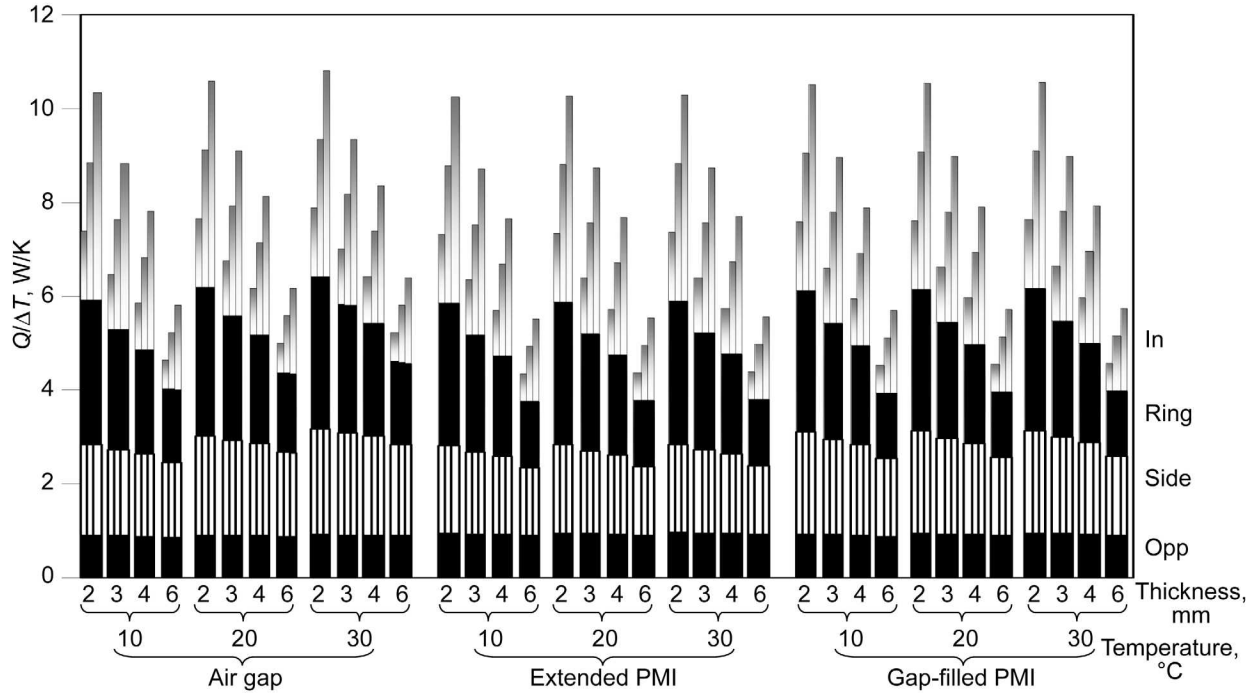


Figure 4.—Stacked bar plots representing the heat divided by ΔT escaping from the heater disc into the sample, the PMI foam ring, the side, and opposite face of the disc as a function of sample thermal conductivity, sample thickness (2.5, 3.2, 3.8, and 6.4 mm), ΔT (10, 20, and 30 °C), and stack side-treatment. Each group of three bars repeatedly represents sample conductivity that is 0.5, 1.0, or 1.5 times that of air ($G = 0.5, 1.0, \text{ or } 1.5$).

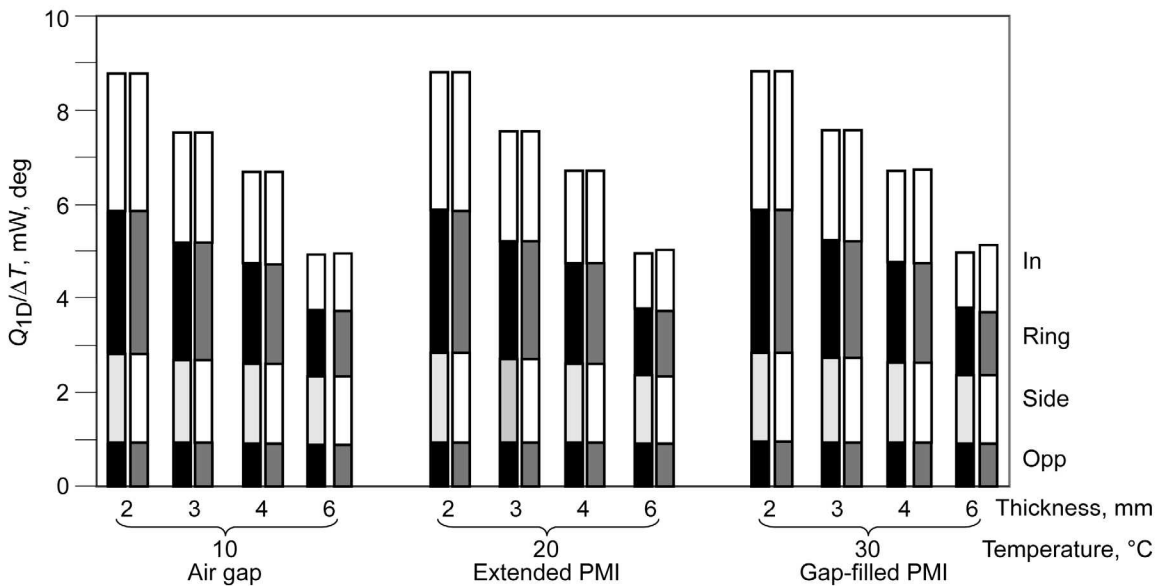


Figure 5.—Stacked bar plots representing the heat divided by ΔT escaping from the heater disc into the sample, the PMI foam ring, the side, and opposite face of the disc as a function of sample thermal conductivity, sample thickness (2.5, 3.2, 3.8, and 6.4 mm), ΔT (10, 20, and 30 °C), and stack side-treatment. Each group of three bars repeatedly represents a solid sample having the same conductivity as air ($G = 1.0$), followed by air.

A portion of the data from the previous two figures may be examined in Figures 6 to 8 to help further support this finding. The parameter $\frac{Q_{1D}}{Q_{in}}$ is equal to one in the ideal case of perfect one-dimensional heat flow through the sample. In this case, the heat entering the sample is precisely the same as the heat expected from the one dimensional heat transfer Eq. (3). Figure 6 illustrates the effect of the stack side-treatment (i.e., air gap versus the extended PMI foam versus the PMI foam-filled gap cases). For visual clarity, only the cases where $\Delta T=20\text{ }^{\circ}\text{C}$ and the conductivity of the solid is equal to that of air are presented. This figure shows that conditions deviate further from one dimensionality as thickness is increased, and that there is a benefit to either extending the PMI foam ring into the gap or in filling the entire gap with PMI foam. There is little difference in the benefits between extending the ring and entirely filling the gap.

In Figure 7, the geometry is held constant—using the extended PMI foam ring case—and the sample conductivity is varied from 0.5 to 1.5 times the conductivity of air, while the value of ΔT is set to 10, 20 or 30 $^{\circ}\text{C}$. The figure shows that, as with Figure 6, the one-dimensionality decreases with increasing thickness and increasing ΔT . But it also shows that $\frac{Q_{1D}}{Q_{in}}$ remains very close to one—for example, it is at or above 0.999 at thicknesses up to 3.8 mm. Even at the thickness of 6.35 mm, the ratio is comfortably above 0.99. However, there is a fairly dramatic fall off at thicknesses above about 4 mm. Figure 8 shows the $\frac{Q_{1D}}{Q_{in}}$ ratio when the solid sample is replaced with air. Here the one dimensionality is not as good as when the sample is a solid due to a small, but not entirely insignificant, amount of additional heat transfer via convection within the sample volume. Furthermore, for the air sample cases, it becomes even more advisable to avoid thicknesses as large as 6.35 mm and to avoid the largest values of ΔT .

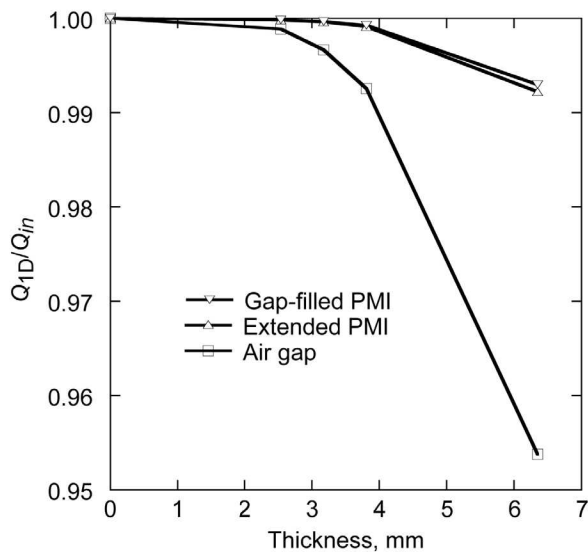


Figure 6.—Effect of stack side treatment (air gap versus extended PMI foam ring versus PMI foam-filled gap) on the one-dimensionality of heat flow through the samples as expressed by Q_{1D}/Q_{in} versus sample thickness for $\Delta T = 20\text{ }^{\circ}\text{C}$ and for conductivity of the solid sample equal to that of air ($G = 1.0$).

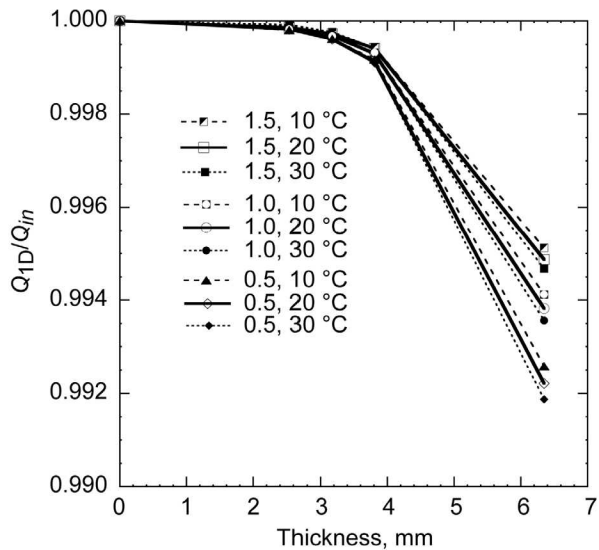


Figure 7.—Effect of three values of conductivity ($G = 0.5$, 1.0, and 1.5) and three values of ΔT on one-dimensionality of heat flow through the solid samples as expressed by Q_{1D}/Q_{in} versus sample thickness.

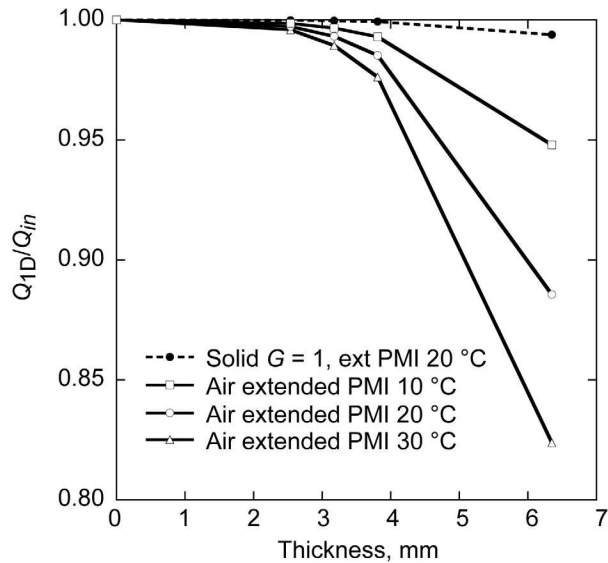


Figure 8.—Effect of replacing solid samples with air on one-dimensionality of heat flow through samples as expressed by Q_{1D}/Q_{in} versus sample thickness for $\Delta T = 10, 20,$ and $30\text{ }^{\circ}\text{C}$. For reference, the plot for a solid sample having conductivity equal to that of air ($G = 1.0$) and $\Delta T = 20\text{ }^{\circ}\text{C}$ is shown.

In summary, heat flow through the sample is more nearly one-dimensional when

- (1) sample thickness is small,
- (2) ΔT is small
- (3) sample conductivity is high
- (4) the sample is a solid rather than air
- (5) the region along the stack side is either fully or partially filled with PMI foam.

Based on the above results and the desire to allow specimens to be as thick as practical, a maximum thickness of 2.5 mm is recommended. However, if the material is not strong enough to cut to this thickness, a 4 mm thickness would be useable.

During a calibration experiment, it would not be possible to bring the experimental temperatures to precisely T_h , T_c , and T_w ; a certain amount of imprecision in the selection of the target temperatures must be permitted. The next round of CFD model calculations was designed to examine how the value of Q_{lost} would be expected to vary within small variations in these three temperatures. The sample thickness was set to 4 mm and the conductivity of the PMI foam was set to 0.032 W/m-K [25]. The solid sample conductivities were again treated as variables and allowed to range from 0.5 to 1.5 times the value of air. The other three variables— T_h , T_c , and T_w —were allowed to vary within the range of 34.5 to 35.5 °C, 14.5 to 15.5 °C, and 24.8 to 25.2 °C, respectively. These should be readily achievable experimental ranges for the three temperature variables. A standard 2^4 Box-Behnken response-surface design [28] was used to systematically place 25 sets of the four variables within the range of interest. A second set of 13 runs, following a 2^3 Box-Behnken design, was used for the case where the sample is replaced with air using the same three temperature variables. Modeled values of Q_{total} and Q_{lost} were recorded for the 25 solid-sample CFD model runs and the 13 air-sample runs for both the non-extended and extended PMI foam case. The PMI foam-filled gap case was not considered because of its strong similarity to the extended PMI foam case.

The regression analyses of the Box-Behnken designs were performed using the commercial code Minitab Version 13 [28]. Before conducting the analysis, the variables were mathematically centered

about the mean values of each variable, i.e., the three temperatures were expressed as $(T_h - 35)$, $(T_c - 15)$ and $(T_w - 25)$. The solid sample conductivities were expressed as 0.5, 1.0 or 1.5 times the thermal conductivity of air, so the centered values were -0.5, 0.0, and 0.5, respectively. One problem with performing a regression analysis on the CFD model data is that the modeled values of Q_{total} and Q_{lost} were calculated to the nearest nanowatt, which is an accuracy far greater than could ever be obtained experimentally. Therefore, in order to more realistically represent experimentally obtainable values, and, thereby, avoid declaring too many variables to be statistically significant, a controlled amount of error was introduced into the model data by truncating the value of Q_{lost} to the nearest 0.1 mW. It will be shown later that this is somewhat better resolution than what was obtained experimentally.

The results of the regression analyses and experimental measurements are shown in Table 2. The first thing to note is that the thermal conductivity term has dropped out of the regression model because it is not statistically significant. This is encouraging because, as described earlier, it implies that a calibration performed using a standard having a given conductivity would hold over the entire range of interest. It is interesting to note that the sum of the coefficients for the T_c and T_w terms are approximately equal to the negative of the coefficient for T_h term. This suggests the possibility of combining the three temperature variables into two differential temperature terms, one of which is Eq. (2), and the other which is:

$$\Delta T_{hw} = (T_h - T_w) \quad (9)$$

A model that uses differential temperatures is attractive because it recognizes that heat may flow from the heater at temperature T_h to either the wall at T_w or cooler disc at T_c . The use of centered terms is preferred for use in regression analysis. The centered ΔT terms may be written as $(T_h - T_c - 20)$ and $T_h - T_w - 10$.

TABLE 2.—RESULTS OF REGRESSION
[Results for Q_{lost} in terms of T_h, T_c, T_w]*

	Model, non-extended solid	Model, non-extended air	Experimental, non-extended air	Model, extended solid	Model, extended air
Constant, α_0	0.10158 (15313)	0.10175 (12874)	0.13786 (4242)	0.092396 (14249)	0.092577 (11142)
$T_h - 35, \alpha_1$	0.00762 (398)	0.00760 (377)	0.00952 (152)	0.00643 (343)	0.00645 (304)
$T_c - 15, \alpha_2$	-0.00362 (189)	-0.00365 (181)	-0.00391 (63)	-0.00288 (154)	-0.00295 (139)
$T_w - 25, \alpha_3$	-0.00379 (79)	-0.00375 (74)	-0.00437 (4)	-0.00308 (66)	-0.00312 (59)
s	0.000033	0.000028	0.000051	0.000032	0.000030
R^2 (adj)	99.99%	99.99%	99.98%	99.98%	99.99%
95% PI (center)	± 0.000067	± 0.000067	± 0.000168	± 0.000069	± 0.000070
95% PI (worst)	± 0.000070	± 0.000078	± 0.000840	± 0.000077	± 0.000082
Number of points	25	25	8	25	25
Constant, β_0	0.10158(12081)	0.10175 (8896)	0.13788 (7549)	0.09240 (6808)	0.09258 (5140)
$(\Delta T - 20), \beta_1$	0.00364(160)	0.00367 (134)	0.00394 (73)	0.00294 (80)	0.00300 (70)
$(\Delta T_{hw} - 10), \beta_2$	0.00395(132)	0.00390 (109)	0.00561 (141)	0.00344 (71)	0.00341 (60)
s	0.000042	0.000041	0.000051	0.000068	0.000065
R^2 (adj)	99.98%	99.99%	99.98%	99.93%	99.95%
95% PI (center)	± 0.00009	± 0.00010	± 0.00014	± 0.00014	± 0.00015
95% PI (worst)	± 0.00011	± 0.00013	± 0.00021	± 0.00018	± 0.00021
Number of points	25	25	8	25	25

*Values in parentheses represent t -values

Postulating that the equation that uses the three centered temperatures is approximately equal to an alternative equation that is written in terms of the two differential temperatures, we may write the following:

$$Q_{lost} = \alpha_0 + \alpha_1(T_h - 35) + \alpha_2(T_c - 15) + \alpha_3(T_w - 25) \quad (10)$$

$$Q_{\text{lost}} \cong \beta_0 + \beta_1(T_h - T_c - 20) + \beta_2(T_h - T_w - 10) \quad (11)$$

$$Q_{\text{lost}} \cong \beta_0 + \beta_1[(T_h - 35) - (T_c - 15)] + \beta_2[(T_h - 35) - (T_w - 25)] \quad (12)$$

$$Q_{\text{lost}} \cong \beta_0 + (\beta_1 + \beta_2)(T_h - 35) - \beta_1(T_c - 15) - \beta_2(T_w - 25) \quad (13)$$

Because the data in each case are centered, $\alpha_0 = \beta_0$. This can be seen by inspecting the table.

Therefore:

$$\alpha_1 \cong \beta_1 + \beta_2 \quad (14)$$

Furthermore,

$$\alpha_2 \cong -\beta_2 \quad (15)$$

and

$$\alpha_3 \cong -\beta_3 \quad (16)$$

which leads to:

$$\alpha_1 \cong -(\alpha_2 + \alpha_3) \quad (17)$$

The latter relationship provided the clue that the three term expression could possibly be replaced by a two term expression in terms of two differential temperatures. In all of the modeled cases above, the regression coefficients on the $(T_c - 15)$ term are indeed approximately equal to the negative of the coefficients on the $(\Delta T - 20)$ term, and the coefficients on the $(T_w - 25)$ term are approximately equal to the negative of the coefficients on the $(T_h - T_w - 10)$ term.

While the two-term differential temperature expressions fit the modeled data quite well, the three term expression fits it better. This model is not expected to have a rigorous physical meaning because of effects such as fringing, in which heat flowing from T_h to T_c may travel an indirect path through the air at the edge of the stack. However, as will be discussed in the next section, there may be cases where it is advantageous to analyze experimentally determined data in terms of the two-term expression.

It is instructive to examine how the coefficients calculated from the data modeled for the air samples may differ from the values calculated for the solid samples. If an air calibration should prove to be feasible, then the regression constants must either be essentially equal to those that would have been attained using a solid sample having the same thermal conductivity, or there must be a rational correction that could be applied. Confidence intervals for the coefficients may be determined using the results of the regression in Table 2. Experimental results corresponding to the non-extended air case are shown in Table 3. The plus or minus limits in Table 2 are obtained by dividing the t -values, given in parentheses in the table, into the coefficient and multiplying the result by the t -statistic for 22 degrees of freedom (25 runs minus the three coefficients). For 95 percent confidence intervals, this t -value is 2.074. The 95 percent confidence intervals for β_0 , β_1 , and β_2 are shown in Table 4 for both the solid and air non-extended PMI foam cases. The confidence interval obtained from the experiment is also shown in Table 4. One may see that β_1 and β_2 —the coefficients on $(\Delta T - 20)$ and $(\Delta T_{hw} - 10)$, respectively,—for the solid non-extended PMI foam case are not statistically different from those two coefficients for the air non-extended PMI foam case. For the constant term β_0 , the confidence intervals do not overlap, so there is a statistically significant difference between the two. The difference between these two β_0 terms is 0.00017 ± 0.000003 , where the plus-or-minus terms for the difference are obtained from the square root of the sum of the squares of the individual terms.

TABLE 3.—REDUCED EXPERIMENTAL DATA—AVERAGE VALUES OF 9000 POINTS

T_w (°C)	T_h (°C)	T_c (°C)	V (Volts)	I (amperes)	P (Watts)	ΔT (°C)	$T_{av} - T_w$ (°C)
24.9959	35.378	15.701	0.071842	2.4391	0.17523	19.677	0.544
25.0087	34.189	14.748	0.070145	2.3818	0.16707	19.442	-0.540
25.0217	34.742	14.104	0.072192	2.4524	0.17704	20.638	-0.598
25.0455	35.644	15.285	0.072891	2.4748	0.18039	20.358	0.419
25.0130	35.036	15.006	0.071836	2.4399	0.17528	20.030	0.008
25.0379	34.431	14.482	0.071035	2.4122	0.17135	19.950	-0.581
25.0115	35.448	15.562	0.072105	2.4510	0.17673	19.886	0.494
25.0456	35.001	15.060	0.071611	2.4350	0.17437	19.940	-0.015

TABLE 4.—NINETY-FIVE PERCENT CONFIDENCE INTERVALS ON THE COEFFICIENTS FOR THE NON-EXT CASES

	Solid, non-extended	Air, non-extended	Experimental, air, non-extended
Range of β_0	0.10156 to 0.10159	0.10172 to 0.10177	0.13784 to 0.13793
Range of β_1	0.00360 to 0.00369	0.00362 to 0.00373	0.00380 to 0.00408
Range of β_2	0.00389 to 0.00401	0.00383 to 0.00398	0.00550 to 0.00571

It is reasonable to assume that the difference between the values of β_0 for the air versus solid sample cases arises from convection in the air-sample region. In the Appendix, we estimated that $h_{conv} = 0.035 \text{ W/m}^2\text{-K}$ for a cross sectional sample area of 0.0002850 m^2 . Therefore, we may estimate that $hA = 0.000010 \text{ W/K}$. Because the data have been centered, β_0 equals the value of Q_{lost} at the center point ($T_h = 35 \text{ }^\circ\text{C}$, $T_w = 15 \text{ }^\circ\text{C}$, $T_c = 25 \text{ }^\circ\text{C}$). Therefore $h_{conv}A\Delta T = 0.00020 \text{ W}$ at the center point. This value of Q_{lost} matches the above difference in coefficients, suggesting that the simple model in the Appendix is describing the heat transfer between the heater and cooler plates in the air sample case. Since $h_{conv}A$ is a coefficient on ΔT , we may expect it should be equal to the difference between the β_1 terms for the air versus solid sample cases. However, the difference in these two regression terms may be written as 0.00003 ± 0.00007 . Therefore, any difference is below the level of detectability.

To summarize, we can correct for the effect of using air as a calibration standard by subtracting 0.0002 from the experimentally determined value of β_0 . We can consider subtracting 0.00001 from the experimentally determined value of β_1 , but this correction would be negligible and not detectable for the small range of ΔT being considered. The correction for radiation across the sample is discussed in the Appendix.

It is constructive to view temperature contours obtained from the model representative temperature contours in the region of the stack and air gap along the side of the stack for three cases are shown in the Figure 9. The temperature of the heater disc is $35.0 \text{ }^\circ\text{C}$ and the cooler disc is $15.0 \text{ }^\circ\text{C}$. The wall temperature is $25.0 \text{ }^\circ\text{C}$ in Figures 9(a) and (b) and $25.3 \text{ }^\circ\text{C}$ in Figure 9(c). The region along the side of the stack is an air gap between the two large PMI foam discs in Figure 9(a), and the PMI foam ring is allowed to extend to the entire diameter of the large PMI foam disc in Figures 9(b) and (c).

Figure 9(a) shows that the contours in the gap region are essentially s-shaped—a result of the convection rolls in that region. The PMI foam ring extending into the gap in Figure 9(b), prevents the formation of convection rolls and, as a result, the contours are more “well behaved”. Note how the $25 \text{ }^\circ\text{C}$ contour near the outside diameter of the stack is initially nearly perpendicular to the side of the stack. However, this contour bends toward the heater due to convection rolls in the air gap region between the large PMI foam disc and the wall, which is also at $25.0 \text{ }^\circ\text{C}$. In Figure 9(c), the wall temperature has been increased to $25.3 \text{ }^\circ\text{C}$, and as a result, the $25.0 \text{ }^\circ\text{C}$ contour is now more nearly vertical. However, when it

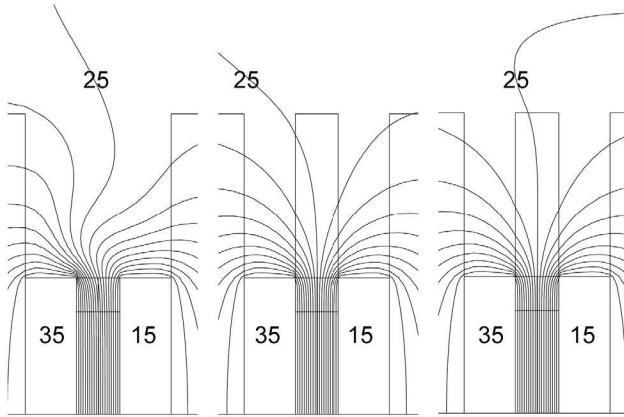


Figure 9.—Modeled temperature contours in the stack and air-gap regions for three cases of T_h , T_w , and T_c , and two different stack side-treatments. (a) Air gap with temperatures of 35.0, 25.0, and 15.0 °C, respectively. (b) Extended PMI foam with temperatures of 35.0, 25.0, and 15.0 °C, respectively. (c) Extended PMI foam with temperatures of 35.0, 25.3, and 15.0 °C, respectively.

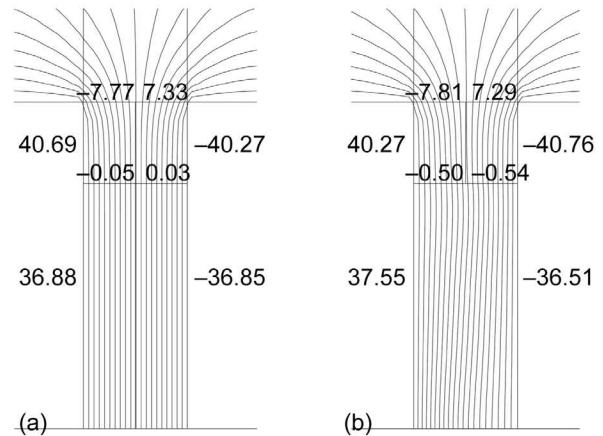


Figure 10.—Modeled temperature contours in the region of the sample and labeled boundary heat flux vectors for two cases, both of which have the extended PMI foam stack side-treatment and temperatures of 35.0, 25.0, and 15.0 °C, respectively. (a) Solid sample having the same conductivity as air (i.e., $G = 1.0$). (b) Air sample. The sign convention used for the heat flux vectors is positive for heat flow towards the sample.

enters into the air region beyond the large PMI foam disc, the contour soon turns sharply towards the direction of the cooler disc. Presumably, at some temperature intermediate between 25.0 and 25.3 °C, the 25.0 °C contour may be essentially perpendicular to the stack along its entire length. This would be the condition when the temperatures along the stack are most balanced. The observation that somewhat higher T_w may lead to more balanced heat flows has been noted in the literature [29, 30]. These two references present expressions for determining the amount the ambient temperature should be raised above the mean of T_h and T_c in order to give the condition where the heat escaping from the heater-side edge of the guard surrounding a sample is equal to the heat that returns to the cooler-side edge of the guard. Using expressions A1.6 through A1.10 of [29], one can show that for the present experiment, the ratio of their $\frac{A}{B}$ terms are approximately equal to the ratio of their $\frac{A'}{B'}$ terms, and the optimum “ambient temperature” increase above the average sample temperature reduces to approximately:

$$T_w - T_{av} = \frac{1}{4} \exp \left[\frac{\pi(d-b)}{l} \right] \Delta T \quad (18)$$

where $(d - b)$ is the outer radius of our stack minus the radius of the sample. (In the standard [29], d refers to the radius of the guard. Here, it refers to the radius of the PMI foam ring, which is a type of guard). $T_w - T_{av}$ is the increase in wall temperature above the average temperature where the heat loss out the top edge of the sample would equal the heat that re-enters the bottom edge. This expression predicts a value of 0.4 °C, which is very close to the value for the optimum increase in T_w determined from the CFD analysis of a little below 0.3 °C. Practically speaking, employing a wall temperature at the mean temperature between the heater- and cooler-disc temperatures should be adequate. However, there does appear to be some advantage to raising the wall temperature by perhaps 0.25 °C relative to this mean temperature.

All three contour plots in Figure 9 are for solid samples. For air samples with the same thermal conductivity, the figures look very much the same, unless they are viewed closely in the sample region. Such views are shown in Figure 10. In Figure 10(b)—a close-up view of the solid case corresponding to

Figure 9(b)—the temperature contours within the sample region appear parallel, indicating essentially one-dimensional heat transfer. The numbers on the plots are the CFD modeled values of the heat transfer across the boundary. Note that heat flux vectors for solids are perpendicular to the temperature contours. The heat leaving the sample is very close to the heat entering, and there is a small amount of heat leaving the heater-side edge of the sample that is mostly returned on the cooler side, the goal of our balanced design. When an air sample is used, a very small convective roll sets up within the sample volume, and the contours, while remaining nearly parallel, are not quite as parallel as they were for the solid case. Now the heat leaving the specimen from the cooler face is somewhat less than the heat entering, and heat is leaving from the edge on both the heater- and cooler-disc side of the sample edge. Therefore, as discussed above, the heat transfer across the 4 mm wide air sample is not perfectly one-dimensional. However, in the absence of suitable small thermal conductivity standard reference materials, it may be preferable to use air as a calibration standard, but to apply small corrections to account for the effects of convection and radiation. Of course, if the sample region can be 2 mm wide or smaller, then air can be used as a calibration standard without the need for much, if any, correction for convection. From the Appendix, the heat transfer from convection is expected to decrease by a factor of 13 if the sample thickness is reduced from 4 to 2 mm. However, either thickness would require the same radiation corrections as for the 4 mm case.

Experimental Results

A series of experiments were conducted to determine if measurements of sufficient precision could be made to allow accurate determination of thermal conductivity, and to demonstrate the feasibility of using air as a calibration standard. The dimensions of this apparatus, discussed in the Experimental Design section, differ from those used to model the “air gap” case in that the diameters of the large PMI foam discs were increased somewhat in order to take further advantage of the thermal insulation provided by the air gap. Also, the thickness of the PMI foam discs were increased by 50 percent in order to allow a firmer attachment to the threaded rods that hold the fixture in place (refer to Figure 1(b)).

The experiments involved measurement of the power required to achieve eight combinations of the three temperatures of interest: T_h , T_c , and T_w . The eight sets of temperatures were spread within the target temperature range of 25 ± 0.2 °C, the cooler temperature range of 15 ± 0.5 °C, and the heater temperature range of 35 ± 0.5 °C. However more care was taken in the selection of T_h and T_c than in the selection of T_w . The measured independent variable for these measurements was Q_{total} . The sample volume in each case was assumed to be filled with air of known thermal conductivity, as it was in the air cases in the previous section.

Matched thermocouples were used for the three critical temperature measurements. A total of 25,000 data points was collected over 640 min. The temperatures, voltage, and amperage were the average of a stable region of 9000 continuous points collected over 230 min. The stable regions tended to be those times when the temperature of the room was essentially stable. By averaging over 9000 points, mean values for temperature, voltage and amperage measurements could be accurately determined. For example, the standard error of the mean for the temperature measurements was less than 0.001 °C, even though the data logger recorded each temperature value to only ± 0.1 °C. It is interesting to note that for this approach to work, the power supply must be sufficiently noisy so as to output an essentially Gaussian distribution of power about the nominal value.

The experimental data and coefficients resulting from the linear regression fit to the data are presented in Tables 3 and part of Table 2, respectively. The experimental data are the averages of the various temperatures and the voltage and current supplied to the heater. Table 3 includes the product of the voltage and current, which is the electrical power in watts (identical to Q_{total}). The regression fits, whether in terms of the centered temperatures or the centered differential temperatures, were linear in terms of these variables in a manner similar to the regression of the modeled data. The t -values associated with most of the coefficients are very high, indicating high significance. The $(T_w - 10)$ term, although significant at a value of 4, is far below the values of t associated with all of the other coefficients in the table. This is because the experiment was not well-designed in terms of the wall temperature. However,

when the wall temperature was incorporated in terms of the differential temperature, ΔT_{hw} , the t -value associated with its coefficient becomes much higher, as shown in the table.

Discussion

Both regression equations fit the data very well with a standard deviation of 0.000051 and an adjusted R^2 of 99.98 percent in both cases. However, the 95 percent prediction interval, which is an important quantity for calibration runs such as these, is better when the data is expressed in terms of the differential temperatures. For the regression in terms of the temperatures, the 95 percent prediction intervals for both the temperature and differential temperatures cases are ± 0.000168 and ± 0.000145 W, respectively, at the center of the design space. At the extremes of the design space, the 95 percent prediction intervals are ± 0.000840 and ± 0.000214 W, respectively. The relatively high “worst-case” value for the prediction interval for the temperature case arises because of the higher uncertainty on the $(T_w - 25)$ term. Fortunately for this data set, the worst-case 95 percent prediction interval is still very tight. It shows that, given a set of differential temperatures near the values of $(\Delta T - 20)$ and $(\Delta T_{hw} - 10)$, we may predict the value of Q_{lost} to ± 0.21 mW or better. In terms of the experimentally measured value of Q_{lost} , this is an error of ± 0.15 percent. Since the various values of Q_{ID} are smaller than Q_{lost} , the error in determining Q_{ID} is greater than the error in determining Q_{lost} . For the case where the conductivity is equal to that of air, the value of Q_{ID} at the center point is calculated to be 0.03684 W. The value of Q_{lost} at the center is equal to 0.137885. Therefore, the error in determining Q_{ID} would be larger than the error in determining Q_{lost} by a factor of $(0.137885 + 0.03684)/0.03684 = 4.72$. For a sample conductivity that is half of that of air, the factor is 8.48. For conductivity 1.5 times that of air the factor is 3.59. Therefore, the expected error due to the error in measuring the electrical power is expected to be ± 1.29 , 0.72, and 0.54 percent for sample conductivities of 0.5, 1.0, and 1.5, respectively. Other errors, such as those associated with measuring the dimensions of the sample would, of course, add to these values.

The above discussion indicates this technique has the potential for high precision. It remains to be shown that the same precision can be repeatedly achieved when the apparatus is torn down and reassembled. This was attempted once and the value of Q_{lost} was found to be within the predicted range. Further trials were not possible because major construction in the laboratory required long-term disassembly of the apparatus.

For the regression analysis of the experimental data, the coefficient on $(T_c - 15)$ approximately equals the coefficient on $(\Delta T - 20)$, as expected based on discussion in the modeling session. However, the coefficient on ΔT_{hw} cannot be compared because the $(T_w - 25)$ term has not been determined to very high precision. The t -value is only 4 (i.e., the standard error is 1/4 of the value of the coefficient). This inaccuracy in determining the coefficient on T_w in the experimental case arises because the values of T_w were varied in a haphazard manner, rather than systematically. However, it was possible to use the same data to accurately determine the coefficients in terms of the differential temperatures $(\Delta T - 20)$ and $(T_h - T_w - 10)$. The sum of those two coefficients equals the coefficient on $(T_h - 35)$ to within about 1 percent, suggesting that the two-term differential temperature model is more forgiving than the three term model.

Note that the coefficient on ΔT determined experimentally is 7 percent larger than the modeled value. The absolute value of their difference is 0.00026. Part of that difference may have been due to the difference between the size of the PMI foam disc used in the experimental design compared to that in the model. Another part is radiation across the air sample. However, if the value $h_{rad} = 0.09$ W/m²-K calculated in the Appendix is reasonably accurate, then $h_{rad}A$ (the radiation contribution to the coefficient on ΔT) is expected to be less than 0.00003 W/K. Thus, radiation may only account for about 10 percent of the difference. Another part of the discrepancy could be heat transfer from the heater disc edge to the coolant tube to the cooler disc, as well as heater wires and sheathed thermocouples coming out of the heater disc. This design could be improved in future versions of the apparatus.

The experimentally determined coefficient on ΔT_{hw} , which, when centered, is expressed as $(\Delta T_{hw} - 10)$, is much higher than the modeled β_2 . The difference is 0.0017, i.e., 44 percent. This discrepancy is partly due to contribution from radiation. We can estimate the magnitude of the heat transfer by radiation off of the large PMI foam disc. For the modeled case from the previous section, the surface area is 0.0073 m^2 . From Eq. (14) in the Appendix, $h_{rad}A \approx 0.0034 \text{ W/K}$, which was obtained using a reasonable guess of $\epsilon=0.8$ for the total emissivity of the PMI foam. From the CFD analysis, the mean surface temperature of the similarly constructed PMI foam disc is $26.0 \text{ }^\circ\text{C}$ which is $1.0 \text{ }^\circ\text{C}$ above the wall temperature. Therefore,

$$h_{rad}A(26 - 25) = 0.034 \text{ W} \quad (19)$$

which is very close to the difference in the β_0 terms between the experiment and the model. Of course, the model did not include radiation. For the experimental case, the surface area of the PMI foam disc is even larger, but the surface temperature would be expected to be lower. Therefore, the same trends should apply.

The difference in β_2 coefficients is 0.0017. The value of $h_{conv}A$ was given as 0.034 W/K . But as, discussed above, the temperature at the surface of the PMI foam disc drops from $35.0 \text{ }^\circ\text{C}$ at the heater to about $26.0 \text{ }^\circ\text{C}$ at the surface of the disc. Calling this latter term T_{surf} , we therefore may write:

$$(T_{surf} - T_w) \approx \frac{1}{10} (\Delta T_{hw}) \quad (20)$$

Therefore, we can expect the convective heat transfer to be approximated as:

$$Q_{conv} = \frac{h_{conv}}{10} (\Delta T_{hw}) \quad (21)$$

The estimated value of $\frac{h_{conv}}{10}$ is $0.00042 \text{ W/m}^2\text{-K}$, which is of the same magnitude as the difference in β_2 coefficients of 0.0017. Again, there are some differences between the modeled and experimental designs. The perturbing effects of the wires, thermocouples and coolant tubes may also contribute to the discrepancy between experiment and the model.

In any event, while it is highly desirable to understand discrepancies between the model and experiment, the experimental calibration equation, not the modeled equation, would be used to determine the value of Q_{lost} . This experimentally determined value would be subtracted from the value of Q_{total} measured for each unknown sample, and the unknown thermal conductivity would be calculated from their difference, Q_{1D} .

Note that no attempt should be made to apply conductive grease at the copper sample interface. This is because air itself is an excellent contact fluid for the conductivities of interest. Also, the application of a thin layer of grease to the polished copper surface will raise its emissivity and allow higher heat transfer by radiation.

For compressible samples, the standards [2-5] allow the sample to be cut slightly oversized, then compressed. It also allows spacers, as we are using. However, for samples that are not compressible, it may be possible to cut them slightly undersized and make the small correction for the air gap. For this strategy, there may be some advantage to using a vertical orientation, where the specimen would lay neatly on the cooler disc with a small air gap between the specimen and the heater disc. It should also be noted that these standards would allow the use of compliant spacers between the heater disc and the specimen in place of an air gap. However, any compliant spacer would likely have a relatively high emissivity and would, therefore, not be usable if we adopt the polished copper plate approach.

Conclusions

The work described in this paper has shown the feasibility of using a hot-plate device that is not guarded—except in the partial sense—for measuring the thermal conductivity of small samples having conductivity on the order of that of air. It also showed that it may well be feasible to use air as a standard reference material, provided that the small amounts of convective and radiative heat transfer are accounted for. Such an approach is desirable because of the lack of suitable small calibration standards.

We conclude that air can be used instead of, for example, a low conductivity powder fill material surrounding the experiment because the effects of convection in the surrounding air can be managed through a design that includes the use of a PMI foam spacer ring that surrounds the sample and which extends to a distance much greater than the diameter of the heater and cooler discs. Furthermore, we conclude that a sample thickness of 0.004 m is feasible, although based on the equations in the Appendix, decreasing the sample thickness from 0.004 to 0.002 m would lower convective heat transfer by 13X, or decreasing to 0.003 m thickness would lower convective heat transfer by 4.5X. Radiative losses would not be affected by thickness. The use of a highly reflective mirror surface—preferably with independent measurement of the emissivity or perhaps even a high-power laser type of mirror optimized for high reflectivity in the mid-infrared—is recommended. Conversely, a second set of measurements could be made using a high emittance surface so that the radiation component to heat transfer could be assessed.

Future improvements could also involve less intrusive cooler lines, heater wires, and thermocouples, as well as a smaller diameter outer aluminum tube to further decrease the convection effects. Also, we feel that the outer insulating box over the chill plate should be replaced by a box with chill plates on all six sides. An outer insulating box may be placed over the box formed from the chill plates. This improved control of the temperature surrounding the apparatus would also permit the removal of the foam blocking the ends of the cylinder. A design incorporating these changes is shown in Figure 1(b). Furthermore, a vertical orientation allowing the test sample to lay flat may prove useful when an intentional air gap between the sample and heater disc is desired.

It has been noted that the obstacles which had to be overcome in developing the approach described in this paper arose primarily because of the very low thermal conductivity of the test samples. In cases where the sample possessed higher conductivity, the task should become easier. For example, thermal barrier coatings can have a thermal conductivity on the order of 1 W/m-K—nearly forty times the thermal conductivity of air. If the same 4 mm thickness used for the experimental part of this study was used, then the heat passing into the sample would have to be increased by the same factor to achieve the same ΔT . However, the thickness of a free-standing thermal barrier coating may be less, such as 0.5 mm, which is 1/8 of the thickness used above. Therefore, the expected value of Q_{in} would only have to be about five times the value used above, or about 0.2 W. This should be much larger than the value of Q_{lost} . It may be possible to use standard or secondary standard reference materials in this thermal conductivity range to determine Q_{lost} .

Although the techniques developed in this study were for single-sided conductivity testing, they are not limited to that approach. For example, these techniques would lend themselves well to a double-sided approach where specimens are placed on both sides of the heater. One of the chief concerns for the double-sided testing had been that the addition of extra layers and an extra PMI foam ring could make alignment more difficult. However the successful use of a spray adhesive to hold portions of the stack together has alleviated those concerns. Another alternative approach, one that employs built-in standards similar to ASTM E1225, should also now be feasible. Again, the use of adhesive would facilitate the alignment of the additional discs and PMI foam rings that would be required. The difficulty in identifying small reference standards has been solved by the use of reference standards comprised of air contained within PMI foam rings and preferably limited to a thickness of 2- or 3-mm. The built-in standards approach requires the use of additional temperature measurements to determine three ΔT values (for the case where a standard is

placed on both sides of the sample). Techniques such as the proposed construction of an isothermal box for stabilizing temperatures combined with the 9000-point averaging appear to have made feasible the measurement of the required extra temperatures. Therefore, we expect that the techniques developed for this study would lend themselves well to the built-in standards approach.

Appendix—Heat Transfer Across a Narrow Vertical Air Gap

Heat transfer across an air gap may occur by conduction, convection, and radiation. For the measurements described in this paper, we wish to minimize the contribution from convection and radiation and to limit heat transfer, to the greatest extent practicable, to conduction. Generally speaking, convection is minimized by a small sample volume and radiation is minimized by the use of highly polished heater and cooler discs.

It is convenient to use effective heat transfer coefficients to characterize each mode of heat transfer [30]:

$$Q = h_{\text{gap}} A \Delta T = (h_{\text{cond}} + h_{\text{conv}} + h_{\text{rad}}) \Delta T \quad (22)$$

where

Q	heat transferred across gap (W)
h_{gap}	overall heat transfer coefficient ($\text{W}/\text{m}^2\text{-K}$)
A	area of the discs (m^2)
h_{cond}	effective heat transfer coefficient for conduction ($\text{W}/\text{m}^2\text{-K}$)
h_{conv}	effective heat transfer coefficient for convection ($\text{W}/\text{m}^2\text{-K}$)
h_{rad}	effective heat transfer coefficient for radiation ($\text{W}/\text{m}^2\text{-K}$)

Since the values of g and ΔT are constants for a given design and set of test conditions, it is instructive to inspect the values of the various heat transfer coefficients.

Following the approach of Takasu, et al. [31] and Ostrach [32], the expression for h_{cond} for the ideal case of one dimensional heat transfer is:

$$h_{\text{cond}} = \frac{k_{\text{air}}}{l} \quad (23)$$

where

l	distance across the gap (m)
-----	-----------------------------

For convection between vertical plates when conduction dominates:

$$h_{\text{conv}} = 0.00166 \left(\frac{l}{H} \right) \text{Gr}^{0.9} \quad (24)$$

where

H	height of the sample area, taken here as the diameter
Gr	Grashof number (dimensionless)

In Eq. (24), the expression for the Grashof number is given by:

$$\text{Gr} = \frac{[\rho^2 g \beta (\Delta T) l^3]}{\mu^2} \quad (25)$$

where

ρ	density of air (kg/m^3)
g	gravitational constant (m/s^2)
β	reciprocal of mean temperature for ideal gases (K^{-1})
μ	viscosity of air ($\text{kg}/\text{m-s}$)

Example calculations may be made for a typical air gap. For a case where the gap width is 0.004 m and the hot and cold discs are 35 and 15 °C, respectively, the value obtained for the conductive heat transfer coefficient is:

$$h_{\text{cond}} = 6.52 \text{ W/m-K} \quad (26)$$

and the convective heat transfer coefficient for $Gr = 170$, which was calculated from Eq. (25), is:

$$h_{\text{conv}} = 0.035 \text{ W/m-K} \quad (27)$$

Thus, the above predicts that convection makes a minor, yet finite, contribution to the overall heat transfer and that more accurate finite volume modeling should be conducted.

Note that this value of Gr is very small. When Gr is multiplied by the Prandtl number, Pr —which is about 0.71 for air at room temperature—their product is:

$$Gr \cdot Pr = 120 \quad (28)$$

This is less than the value of 1708 quoted [33] for the onset of convection, illustrating that we are correcting for contributions due to convection which are so small that they are typically ignored.

For the contribution due to radiation, the expression for h_{rad} for parallel discs having equal total emissivities ϵ is:

$$h_{\text{rad}} = \frac{\sigma(T_h^2 + T_c^2)(T_h + T_c)}{\left(\frac{2}{\epsilon} - 1\right)} \quad (29)$$

Where:

σ Stefan-Boltzman constant ($\text{W/m}^2\text{-K}^4$)

Note that h_{rad} is independent of the plate separation, l .

For T_h approximately equal to T_c and, therefore, approximately equal to their mean, T_{av} , one may write:

$$h_{\text{rad}} = \frac{4\sigma T_{av}^3}{\left(\frac{2}{\epsilon} - 1\right)} \quad (30)$$

If we assume that the plates have been polished so as to have a total emissivity of $\epsilon=0.06$ at a temperature of T_{av} , which appears to be a reasonable value for well, but imperfectly polished copper, then the effective heat transfer coefficient for radiation is estimated to be:

$$h_{\text{rad}} = 0.092 \text{ W/m-K} \quad (31)$$

This is predicted to be a somewhat greater contributor to the heat transfer than convection. Therefore, we must more extensively examine the effect of radiation on this problem in the future, and furthermore, to consider the alternative approach of coating the discs for high emittance so that the radiation contribution would be maximized, but accurately predicable.

References

1. Zarr, R.R., *A History of Testing Heat Insulators at the National Institute of Standards and Technology*. ASHRAE Transactions, 2001. **107 Pt. 2(2)**: p. 111.
2. *ASTM C177-04 Standard Method for Steady-State Heat Flux Measurements and Thermal Transmission Properties by Means of the Guarded Hot Plate Apparatus*. 2004.
3. *ISO 8302:1991 Thermal Insulation—Determination of Steady-State Thermal Resistance and Related Properties—Guarded Hot Plate Apparatus*. 1991.
4. *ASTM C 518-04 Standard Test Method for Steady-State Thermal Transmission Properties by Means of the Heat Flow Meter Apparatus*. 2004.
5. *ISO 8301:1991 Thermal Insulation—Determination of Steady-State Thermal Resistance and Related Properties—Heat Flow Meter Apparatus*. 1991.
6. *ASTM E1225-04 Standard Test Method for Thermal Conductivity of Solids by Means of the Guarded Comparative-Longitudinal Heat Flow Technique*. 2004.
7. Pratt, A.W., *Heat Transmission in Low Conductivity Materials*, in *Thermal Conductivity*, R.P. Tye, Editor. 1968, Academic Press: New York. p. 301–305.
8. Salmon, D., *Thermal Conductivity of Insulations Using Guarded Hot Plates, Including Recent Developments and Sources of Reference Materials*. Measurement Science and Technology, 2001. **12(12)**: p. R89–R98.
9. Zarr, R.R. and J.J. Filliben, *International Comparison of Guarded Hot Plate Apparatus Using National and Regional Reference Materials*. 2002: NIST TN 1444.
10. Zarr, R.R., M.K. Kumaran, and E.S. Lagergren, *NIST/NRC-Canada Interlaboratory Comparison of Guarded Hot Plate Measurements*. NISTIR 6087, 1997.
11. Zarr, R.R., D.R. Flynn, J.W. Hettenhouser, N.J. Brandenburg, and W.M. Healy. *Fabrication of a Guarded-Hot-Plate Apparatus for Use Over an Extended Temperature Range and In A Controlled Gas Atmosphere*. in *International Thermal Conductivity 28th Conference/International Thermal Expansion 16th Symposium Proceedings, June 26–29, 2005*. 2005. New Brunswick, Canada: DEStech Publications, Inc.
12. Lide, D.R., *A Century of Excellence in Measurements, Standards, and Technology*. 2002: CRC Press, Boca Raton, FL.
13. Bennex, R., *Summary of Error Analysis for the National Bureau of Standards: 10016 mm Guarded Hot Plate and Considerations Regarding Systematic Error for the Heat Flow Meter Apparatus*, in *Guarded Hot Plate and Heat Flow Meter Methodology, ASTM STP 879*. 1985, American Society for Testing and Materials: Philadelphia. p. 69–85.
14. Flynn, D.R. and R. Gorthala, *Thermal Design of A Miniature Guarded Hot Plate Apparatus*, in *Insulation Materials: Testing and Applications, ASTM STP 1320*, R.R.Z. R.S. Graves, Editor. 1997, American Society for Testing and Materials: West Conshohocken, PA.
15. Flynn, D.R. and R. Gorthala, *Design of a Subminiature Guarded Hot Plate Apparatus*, in *Thermal Conductivity 23*, R.B.D. Kenneth Earl Wilkes, Ronald S. Graves, Editor. 1996.
16. Meador, M.A.B., E.F. Fabrizio, F. Ilhan, A. Dass, G. Zhang, P. Vassilaras, J.C. Johnston, and N. Leventis, *Crosslinking Amine-Modified Silica Aerogels with Epoxies: Mechanically Strong Lightweight Porous Materials*. Chem. Mater., 2005(17): p. 1085–1098.
17. Dickinson, H.C. and M.S.V. Dusen, *The Testing of Thermal Insulators*. ASRE J., vol. 3(2), 1916, p. 5–25.
18. Michels, A. and A. Boltzen, *A Method for the Determination of the Thermal Conductivity of Gases at High Pressures*. Physica, 1952. **18(8–9)**: p. 605–612.
19. Michels, A., J.V. Sengers, and P.S.V.D. Gulik, *The Thermal Conductivity of Carbon Dioxide in the Critical Region. I. The Thermal Conductivity Apparatus*. Physica, 1962. **28**: p. 1201–1215.
20. Michels, A., J.V. Sengers, and P.S.V.D. Gulik, *The Thermal Conductivity of Carbon Dioxide in the Critical Region. II. Measurements and Conclusions*. Physica, 1962. **28**: p. 1216–1237.

21. Michels, A. and J.V. Sengers, *The Thermal Conductivity of Carbon Dioxide in the Critical Region. III. Verification of the Absence of Convection*. Physica, 1962. **28**: p. 1238–1264.
22. Fesmire, J.E., S.D. Augustynowicz, K.W. Heckle, and B.N. Scholtens, *Equipment and Methods for Cryogenic Thermal Insulation Testing*. Adv. Cryog. Eng., 2004. **49**: p. 579–586.
23. Fesmire, J.E. and S.D. Augustynowicz, *Methods of Testing Thermal Insulation and Associated Test Apparatus*. 2004: US Patent 6,742,926, June 1, 2004.
24. Lu, X., M.C. Arduini-Schuster, J. Kuhn, O. Nilsson, J. Fricke, and R.W. Pekala, *Thermal Conductivity of Monolithic Organic Aerogels*. Science, 1992. **255**(5047): p. 971–972.
25. *Rohm Technical Products - Rohacell Polymethacrylimide Rigid Foam; Rohacell Technical Information*. ca 1986.
26. FLUENT® software from ANSYS, Inc. (www.ansys.com), based in Canonsburg, Pa.
27. Holman, J.P., *Heat Transfer*. eighth ed. 1997, New York: McGraw-Hill, p. 646.
28. *Minitab User's Guide 2: Data Analysis and Quality Tools Release 13 for Windows*. Feb., 2000, State College, PA, pp. 20-5–20-17.
29. *ASTM C1043-06 Standard Practice for Guarded-Hot-Plate Design Using Circular Line Heat Sources*. 2006.
30. Peavey, B. and B.G. Rennex, *Circular and Square Edge Effect Study for Guarded Hot Plate and Heat Flow Meter Apparatus*. Journal of Thermal Insulation, 1986. **9**: p. 254–300.
31. Takasu, T., R.T.C. Choo, R.A. Bergman, and J.M. Toguri, *Thermal Modeling of Air Gaps on the Cooling Capacity of Finger coolers in An Electric Smelting Furnace*. Canadian Metallurgical Quarterly, 2000. **39**(4): p. 455–474.
32. Ostrach, S., *Natural Convection in Enclosures*. Advances in Heat Transfer, 1972. **8**: p. 161–227.
33. Incropera, F.P. and D.P. DeWitt, *Fundamentals of Heat and Mass Transfer, 4th edition*. 1996, John Wiley & Sons: New York. p. 509.

REPORT DOCUMENTATION PAGE			Form Approved OMB No. 0704-0188		
<p>The public reporting burden for this collection of information is estimated to average 1 hour per response, including the time for reviewing instructions, searching existing data sources, gathering and maintaining the data needed, and completing and reviewing the collection of information. Send comments regarding this burden estimate or any other aspect of this collection of information, including suggestions for reducing this burden, to Department of Defense, Washington Headquarters Services, Directorate for Information Operations and Reports (0704-0188), 1215 Jefferson Davis Highway, Suite 1204, Arlington, VA 22202-4302. Respondents should be aware that notwithstanding any other provision of law, no person shall be subject to any penalty for failing to comply with a collection of information if it does not display a currently valid OMB control number.</p> <p>PLEASE DO NOT RETURN YOUR FORM TO THE ABOVE ADDRESS.</p>					
1. REPORT DATE (DD-MM-YYYY) 01-06-2009		2. REPORT TYPE Technical Memorandum		3. DATES COVERED (From - To)	
4. TITLE AND SUBTITLE Method for Measuring Thermal Conductivity of Small Samples Having Very Low Thermal Conductivity			5a. CONTRACT NUMBER		
			5b. GRANT NUMBER		
			5c. PROGRAM ELEMENT NUMBER		
6. AUTHOR(S) Miller, Robert, A.; Kuczmariski, Maria, A.			5d. PROJECT NUMBER		
			5e. TASK NUMBER		
			5f. WORK UNIT NUMBER WBS 984754.02.07.03.16.02		
7. PERFORMING ORGANIZATION NAME(S) AND ADDRESS(ES) National Aeronautics and Space Administration John H. Glenn Research Center at Lewis Field Cleveland, Ohio 44135-3191			8. PERFORMING ORGANIZATION REPORT NUMBER E-16681		
9. SPONSORING/MONITORING AGENCY NAME(S) AND ADDRESS(ES) National Aeronautics and Space Administration Washington, DC 20546-0001			10. SPONSORING/MONITOR'S ACRONYM(S) NASA		
			11. SPONSORING/MONITORING REPORT NUMBER NASA/TM-2009-215460		
12. DISTRIBUTION/AVAILABILITY STATEMENT Unclassified-Unlimited Subject Category: 27 Available electronically at http://gltrs.grc.nasa.gov This publication is available from the NASA Center for AeroSpace Information, 301-621-0390					
13. SUPPLEMENTARY NOTES					
14. ABSTRACT This paper describes the development of a hot plate method capable of using air as a standard reference material for the steady-state measurement of the thermal conductivity of very small test samples having thermal conductivity on the order of air. As with other approaches, care is taken to ensure that the heat flow through the test sample is essentially one-dimensional. However, unlike other approaches, no attempt is made to use heated guards to block the flow of heat from the hot plate to the surroundings. It is argued that since large correction factors must be applied to account for guard imperfections when sample dimensions are small, it may be preferable to simply measure and correct for the heat that flows from the heater disc to directions other than into the sample. Experimental measurements taken in a prototype apparatus, combined with extensive computational modeling of the heat transfer in the apparatus, show that sufficiently accurate measurements can be obtained to allow determination of the thermal conductivity of low thermal conductivity materials. Suggestions are made for further improvements in the method based on results from regression analyses of the generated data.					
15. SUBJECT TERMS Thermal conductivity; Aerogel; Computational fluid dynamics					
16. SECURITY CLASSIFICATION OF:			17. LIMITATION OF ABSTRACT UU	18. NUMBER OF PAGES 30	19a. NAME OF RESPONSIBLE PERSON STI Help Desk (email:help@sti.nasa.gov)
a. REPORT U	b. ABSTRACT U	c. THIS PAGE U			19b. TELEPHONE NUMBER (include area code) 301-621-0390

